ELSEVIER

Catalysis Today 53 (1999) 395–406

CATALYSIS TODAY

www.elsevier.com/locate/cattod

Kinetics of ethane hydrogenolysis over supported platinum catalysts

R.D. Cortright, R.M. Watwe, B.E. Spiewak[1], J.A. Dumesic*

Department of Chemical Engineering, University of Wisconsin, Madison, WI 53706, USA

Abstract

Results of reaction kinetic, microcalorimetric, spectroscopic, and quantum chemical studies are combined to develop a quantitative description of ethane hydrogenolysis over platinum. This work builds on investigations by John H. Sinfelt and co-workers of ethane hydrogenolysis over Group VIII metals. In the present analysis, quantum chemical methods are used to estimate energetics for interactions of various C_2H_x species with platinum that have been observed experimentally in microcalorimetric and spectroscopic studies of ethylene and acetylene adsorption on platinum catalysts. These theoretical methods are then extended to predict energetics for hydrocarbon species and transition states on platinum that can not be observed experimentally. The combined results of these experimental and theoretical investigations provide thermodynamic information about adsorbed C_2 species on platinum as well as transition states for cleavage of the C–C bond in these species. These results were used to refine and constrain kinetic analyses of kinetic data collected for ethane hydrogenolysis over a wide range of conditions. Results of these analyses suggest that the primary reaction pathways for cleavage of the C–C bond take place through activated complexes based on ethyl (C_2H_5) and ethylidene ($CHCH_3$) species. Furthermore, these analyses suggest that while the more abundant surface species (e.g., adsorbed atomic hydrogen, ethylidyne, and vinylidene species) are not directly involved in the primary reaction pathways, they affect the observed kinetic rates through blocking of sites.

1. Introduction

Ethane hydrogenolysis is a probe reaction employed by John H. Sinfelt and co-workers to investigate the reactivities of various metal catalysts (e.g., [1–4]). In these studies, Sinfelt and co-workers conducted analyses of kinetic data to elucidate the nature of the rate determining step and the important reactive species involved in ethane hydrogenolysis. Initially, these investigators utilized the kinetic analysis of Cimino, Boudart, and Taylor [5], based on the following reaction scheme:

$$C_2H_6 \rightleftharpoons C_2H_x(\text{ads}) + ((6-x)/2)H_2$$

$$C_2H_x(\text{ads}) + H_2 \rightarrow CH_4$$

where the first step is quasi-equilibrated and the second step is irreversible. This scheme leads to a rate expression of the power law form:

$$\text{rate} = k P_E^n P_H^{1-na} \quad (1)$$

where a is equal to $(6-x)/2$ and P_E and P_H are the partial pressures of ethane and hydrogen, respectively. Sinfelt [3,4] later conducted kinetic analyses based on a more general reaction scheme involving non-equilibrated adsorption of ethane to form adsorbed hydrogen and C_2H_5(ads) species, followed by quasi-equilibrated dehydrogenation of C_2H_5(ads) to form the adsorbed reactive intermediate C_2H_x(ads) which decomposes to C_1(ads) fragments on the surface:

$$C_2H_6 \rightleftharpoons C_2H_5(\text{ads}) + H(\text{ads}) \rightleftharpoons C_2H_x(\text{ads}) + ((6-x)/2)H_2$$

$$C_2H_x(\text{ads}) \rightarrow C_1(\text{ads})\text{fragments} \rightarrow CH_4$$

* Corresponding author. Tel.: +1-608-262-1095; fax: +1-608-262-5434.

[1] Present address. 3M Corporation, St. Paul, MN 55144, USA.

0920-5861/99/$ – see front matter
PII: S0920-5861(99)00133-9

This reaction scheme leads to the following rate expression:

$$\text{rate} = \frac{k_1 P_{\mathrm{E}}^{n}}{(1 + b P_{\mathrm{H}}^{a})} \quad (2)$$

where $b = k_{-1}/k_3 K$. In this case k_1 and k_{-1} refer to the forward and reverse rate constants for the dissociative adsorption of ethane, respectively, k_3 is the rate constant for the decomposition of C_2H_x(ads), and K is the equilibrium constant for the quasi-equilibrated dehydrogenation of C_2H_5(ads) to form C_2H_x(ads) species. Sinfelt [3,4] used this rate expression to analyze ethane hydrogenolysis kinetic data for a variety of metal catalysts, and the fitted values of n and a were used to estimate the values of x for the C_2H_x(ads) reactive intermediates on these metals.

Ethane hydrogenolysis continues to be the subject of research, as investigators further refine and elucidate the interactions of hydrocarbons with metal surfaces [6–16]. The results of these studies have led to various mechanisms for ethane hydrogenolysis, involving details such as competitive adsorption of hydrogen and splitting of the C–C bond through interaction with either gaseous dihydrogen, surface atomic hydrogen, or vacant surface sites (as reviewed by Shang and Kenney [16]).

Results from kinetic analyses by Sinfelt and co-workers of ethane hydrogenolysis over Pt suggested that the rate-limiting step may involve highly dehydrogenated C_2H_x(ads) species (e.g., $x = 0$) [3]. More recent results of NMR investigations conducted by Klug et al. [17] in conjunction with Sinfelt suggest that the C–C bond breaking step may involve an adsorbed species with $x = 3$ over platinum. In this more recent investigation, it was demonstrated that ethylidyne (CCH_3) species form upon adsorption of acetylene on platinum, and it was suggested that these ethylidyne species may play a role in the C–C bond scission of acetylene [17]. These results for ethane hydrogenolysis illustrate the general difficulty in using analyses of reaction kinetics data alone to elucidate the nature of reaction mechanisms. This present paper illustrates how additional information about reaction mechanisms can be obtained by combining data from diverse experimental techniques with results from quantum chemical calculations which are capable of predicting structures and energetics for possible reaction intermediates and transition states.

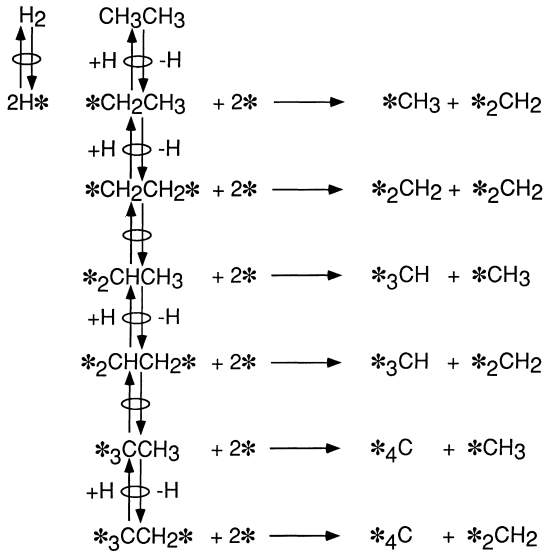

Fig. 1. Proposed reaction pathways for ethane hydrogenolysis over platinum.

In the present study, we have utilized the ethane hydrogenolysis reaction scheme shown in Fig. 1 to describe the combined results of recent kinetic, microcalorimetric, spectroscopic, and theoretical investigations of the interactions of hydrogen and C_2 hydrocarbons with platinum. This reaction scheme is based on several generally accepted aspects of ethane hydrogenolysis over platinum [11]. In particular,

1. hydrogen is adsorbed dissociatively on the Pt surface;
2. ethane is adsorbed dissociatively, undergoing cleavage of a C–H bond;
3. further dehydrogenation of the adsorbed alkyl species occurs, accompanied by the creation of additional bonds between the C_2H_x(ads) species and the metal surface;
4. the C–C bond breaks and CH_y(ads) and CH_z(ads) species are produced;
5. hydrogenation of the CH_y(ads) and CH_z(ads) species takes place, followed by desorption of methane.

We have assumed in our analyses that the dissociative adsorption of dihydrogen and the dissociative adsorption of ethane to form various C_2H_x(ads) species are quasi-equilibrated processes. The quasi-equilibrated adsorption of ethane to form C_2H_x(ads) species on platinum surface is reasonable

since deuterium tracing experiments show that exchange reactions between ethane and deuterium to yield deuterated ethane occur at higher rates than the hydrogenolysis reaction. In particular, Zaera and Somorjai [18] showed that the deuterium exchange rates were 3-orders of magnitude faster than the rate of ethane hydrogenolysis over Pt(111) at temperatures between 475 and 625 K.

The quasi-equilibrated adsorption of both dihydrogen and ethane leads to a particularly convenient framework for writing the reaction scheme for ethane hydrogenolysis. Specifically, we may write the formation of C_2H_x(ads) species in terms of gaseous C_2H_6 and H_2, and these lumped equilibria do not involve assumptions about the strength or mobility of adsorbed hydrogen atoms. Thus, we write the formation of stable adsorbed species as:

$$\text{Step 1}\quad H_2 + 2* \rightleftharpoons 2H*$$

$$\text{Step 2}\quad C_2H_6 + (6-x)* \rightleftharpoons C_2H_x *_{6-x} + ((6-x)/(2))H_2$$

Another important implication of the quasi-equilibrated adsorption of dihydrogen and ethane is that we may also write lumped equilibria involving gaseous C_2H_6 and H_2 with activated complexes for C–C bond cleavage of the various C_2H_x(ads) reactive intermediates. The activated complex for C–C bond cleavage of a particular C_2H_x(ads) species is in equilibrium with that C_2H_x(ads) species according to transition state theory, and as noted above, the C_2H_x(ads) reactive intermediates are in equilibrium with gaseous C_2H_6 and H_2. Therefore, we first use transition state theory to write the formation of activated complexes for the different C–C bond cleavage steps given in Fig. 1 in terms of equilibria involving C_2H_x(ads) species:

$$\text{Step 3}\quad C_2H_x *_{6-x} + 2* \rightleftharpoons [C_2H_x *_{8-x}]^{\ddagger} \rightarrow C_1 \text{ Products}$$

where $\left[C_2H_x *_{8-x}\right]^{\ddagger}$ is the activated complex. Combination of Steps 1, 2, and 3 then leads to the quasi-equilibrated formation of a particular activated complex from gas-phase ethane with the formation of gas-phase dihydrogen as shown in Step 4.

$$\text{Step 4}\quad C_2H_6 + (8-x)* \rightleftharpoons [C_2H_x *_{8-x}]^{\ddagger} + ((6-x)/(2))H_2$$

According to Step 4, the surface coverage of a particular activated complex necessary for C–C cleavage of C_2H_x(ads) can be expressed in terms of the equilibrium constant to form the activated complex ($K_x^{\ddagger}$) and the partial pressures of ethane (P_E) and dihydrogen (P_H) as shown in Eq. (3):

$$\theta_{[C_2H_x *_{8-x}]^{\ddagger}} = \frac{K_x^{\ddagger} P_E \theta_*^{8-x}}{P_H^{6-x/2}} \tag{3}$$

where θ_* is the fractional coverage of free sites. The advantage of expressing the formation of the activated complexes in terms of gaseous C_2H_6 and H_2 is that these lumped equilibria do not involve assumptions about the strengths or mobilities of C_2H_x(ads) species and adsorbed hydrogen atoms.

The rate of a given elementary step is equal to the concentration of the activated complex times a frequency factor equal to k_BT/h, where k_B is Boltzmann constant, T is the temperature, and h is Planck's constant. Therefore, the rate expression for the C–C bond cleavage of a given activated complex may be given by Eq. (4), which is a function of the partial pressures of gas-phase ethane, gas-phase dihydrogen, and the fractional coverage of free sites.

$$\text{rate}_x = \frac{k_B T}{h}\theta_{[C_2H_x *_{8-x}]^{\ddagger}} = \frac{k_B T}{h}\frac{K_x^{\ddagger} P_E \theta_*^{8-x}}{P_H^{6-x/2}} \tag{4}$$

The fractional coverage of the surface not covered by stable C_2H_x(ads) or adsorbed atomic hydrogen is expressed by a site balance given in Eq. (5):

$$\theta_* = 1 - \theta_H - \sum_{x=2}^{5}(6-x)\theta_x \tag{5}$$

where θ_H and θ_x are given by:

$$\theta_H = \sqrt{K_H P_H}\,\theta_* \tag{6}$$

$$\theta_x = \frac{K_x P_E \theta_*^{6-x}}{P_H^{6-x/2}} \tag{7}$$

The present paper utilizes Eqs. (4)–(7) to consolidate the combined results from experimental [19–21] and theoretical investigations [22,23] with the aim to interpret the observed reaction kinetics data for ethane hydrogenolysis collected over a wide range of conditions. The results of spectroscopic and microcalorimetric investigations provide information about the

nature and energetics of adsorbed hydrogen as well as various stable C_2H_x(ads) species on platinum [19–21]. Importantly, these experimental investigations of stable surface species are complimented with quantum chemical calculations which predict the energetics of these experimentally observed C_2 hydrocarbons on Pt and which predict the energetics of species that cannot be observed experimentally [22]. Furthermore, these theoretical methods are used to estimate the energetics of transition states involved in C–C bond cleavage for various C_2H_x(ads) species [23], and these quantum chemical calculations, therefore, provide the means for taking full advantage of the lumped transition state equilibria expressed by Step 4.

2. Summary of experimental and theoretical studies

As noted above, the strategy of our study of ethane hydrogenolysis over platinum was to collect reaction kinetic data over a wide-range of reaction conditions, and to combine these data with results of experimental and theoretical investigations which probe the nature, energetics, and reactivities of various C_2H_x(ads) species on platinum. This present paper specifically reports the reaction kinetic data collected over a wide range of conditions as well as the kinetic analyses of this data. These kinetic analyses utilize results from recent experimental [19–21] and theoretical investigations [22,23], which are summarized briefly below.

2.1. Kinetic data for ethane hydrogenolysis over Pt

A 2.5 wt.% Pt (analyzed by Galbraith Laboratories) catalyst was prepared by ion-exchange of platinum on Cab-O-Sil EH-5 (Cabot), using the method of Benesi et al. [24]. The resulting material was filtered, washed with deionized water, and dried overnight in air at 390 K. Hydrogen chemisorption indicated that this catalyst contained 110 μmol/g of surface Pt atoms (corresponding to a Pt dispersion of 0.85).

Reaction kinetic studies of ethane hydrogenolysis were conducted using a quartz, down-flow reactor. Helium (Liquid Carbonic) was employed as a carrier gas, and it was purified by passage through copper turnings at 473 K, followed by activated molecular sieves (13X) at 77 K. Ethane (Liquid Carbonic, 99.5%) was treated by passage over beds of reduced Oxytrap (Alltech) at 298 K to remove oxygen impurities. Hydrogen (Liquid Carbonic) was treated by passage through a Deoxo unit (Engelhard) and a bed of molecular sieves (13X) at 77 K. The reactor inlet and outlet gases were analyzed by a HP-5890 gas-chromatograph with FID detector and a 7 ft 0.19% Picric Acid Graphpac GC 80/100 column held at 303 K. Turnover frequencies were calculated from the kinetic data based on the number of surface platinum atoms determined by hydrogen chemisorption.

Reaction rates and pressure dependencies for ethane hydrogenolysis were determined over the silica-supported Pt catalyst at 573, 623, and 673 K. These kinetic data were collected with the catalyst in a substantially clean state using the technique employed by Bond and Cunningham [7]. Furthermore, this sampling procedure is similar to the methods employed by Sinfelt and co-workers [1–4]. The kinetic procedure of the present study consisted of first reducing the catalyst at 723 K for 1 h in flowing hydrogen. The temperature was then decreased to the desired reaction temperature in flowing hydrogen and the reactor was bypassed. Helium and ethane were mixed at the appropriate flow-rates to achieve the desired partial pressures of ethane and hydrogen. The reactant gases were allowed to pass over the catalyst for a period of 1 min, at which time the reactant effluent was sampled using a six-port sample valve. After sampling, the ethane flow was stopped, and the catalyst was treated in flowing hydrogen for 15 min at the reaction temperature. The reactor was then bypassed and helium and ethane were mixed at a new set of conditions. All data were collected at a total flow-rate of 304 cm^3/min (STP) and the catalyst amounts were adjusted to maintain ethane conversions less than 30%. Sieved catalyst fractions (80–120 mesh) of the various platinum-based catalysts were employed to ensure that the rates were not influenced by transport limitations [25–27].

Figs. 2–5 show the change of the methane production rate with respect to the ethane and hydrogen pressures at 573, 623, and 673 K. Tests were conducted at replicate conditions to track possible changes in catalyst reactivity (e.g., deactivation). Data points for these replicate tests are shown in Figs. 2–5. Fig. 2 shows a negative hydrogen pressure dependence at an ethane pressure of 0.0066 atm, with hydrogen orders near

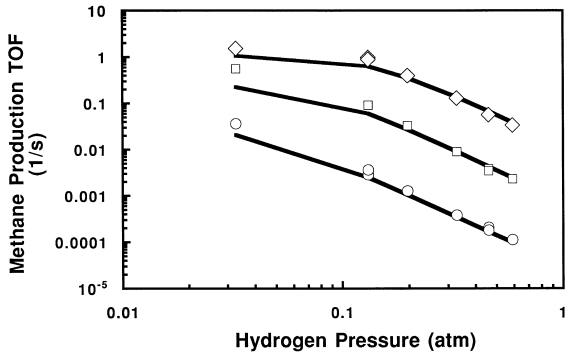

Fig. 2. Hydrogen pressure dependencies for ethane hydrogenolysis at 0.0066 atm ethane pressure [experimental results: ○, 573 K; □, 623 K; and ◇, 673 K]. Predicted rates given by solid line.

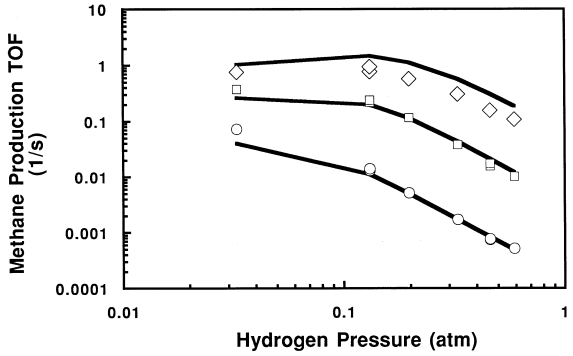

Fig. 3. Hydrogen pressure dependencies for ethane hydrogenolysis at 0.033 atm ethane pressure [experimental results: ○, 573 K; □, 623 K; and ◇, 673 K]. Predicted rates given by solid line.

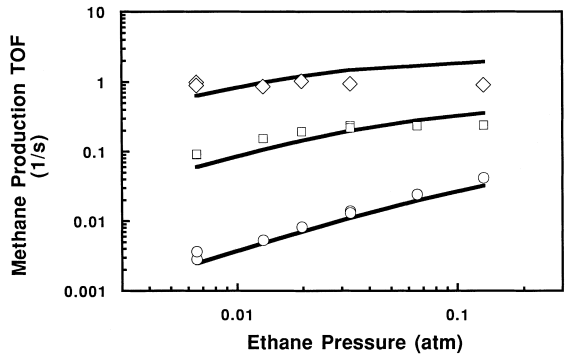

Fig. 4. Ethane pressure dependencies for ethane hydrogenolysis at 0.13 atm hydrogen pressure [experimental results: ○, 573 K; □, 623 K; and ◇, 673 K]. Predicted rates given by solid line.

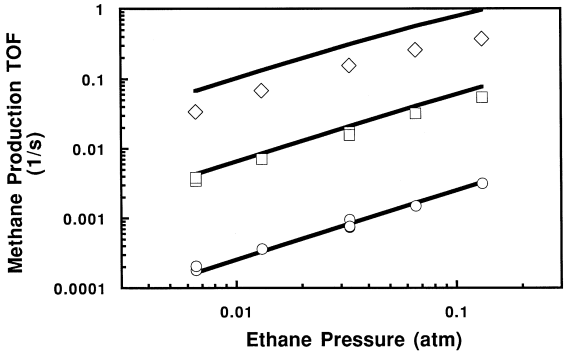

Fig. 5. Ethane pressure dependencies for ethane hydrogenolysis at 0.46 atm hydrogen pressure [experimental results: ○, 573 K; □, 623 K; and ◇, 673 K]. Predicted rates given by solid line.

−2.3 at hydrogen pressures between 0.2 and 0.6 atm. Sinfelt and co-workers reported a similar hydrogen order (−2.5) over silica supported platinum at comparable reaction conditions [3,4]. Furthermore, this figure shows that the hydrogen orders become less negative at lower hydrogen pressures and higher temperatures. At an ethane pressure of 0.033 atm, Fig. 3 shows a maximum rate with increasing hydrogen pressure at 673 K. This figure shows a hydrogen pressure dependence near −2.2 at hydrogen pressures between 0.2 and 0.6 atm at 573 and 623 K, but it shows a hydrogen order near −1.6 over this pressure range at 673 K. Gudkov et al. [13] also observed a maximum rate over silica-supported platinum with increasing hydrogen pressure at higher ethane pressures and reaction temperatures.

Fig. 4 shows that the ethane pressure dependence decreases from ca. 1.0 to 0.0 as the temperature increases from 573 to 673 K for a hydrogen pressure of 0.13 atm. In contrast, Fig. 5 shows that the ethane kinetic orders are near unity at all temperatures for a higher hydrogen pressure of 0.46 atm.

2.2. Microcalorimetric studies of hydrogen adsorption on platinum

The energetics for the dissociative adsorption of hydrogen on a number of platinum surfaces have been determined by calorimetric methods [11,19,21,28–30]. Fig. 6 shows a plot of the differential heat for hydrogen adsorption versus the fractional surface coverage of hydrogen on a 1.2 wt.% Pt/SiO_2 catalyst at 403 K [21]. The differential heat (kJ/mol) is defined as the

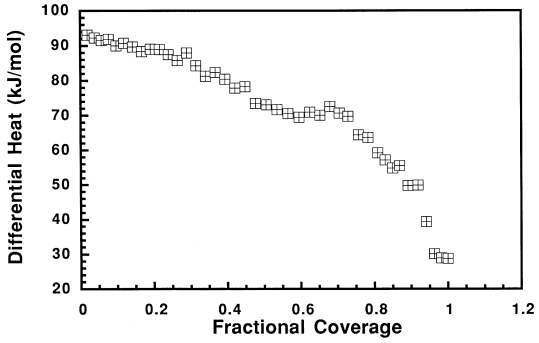

Fig. 6. Differential heats of hydrogen adsorption on silica-supported platinum at 403 K.

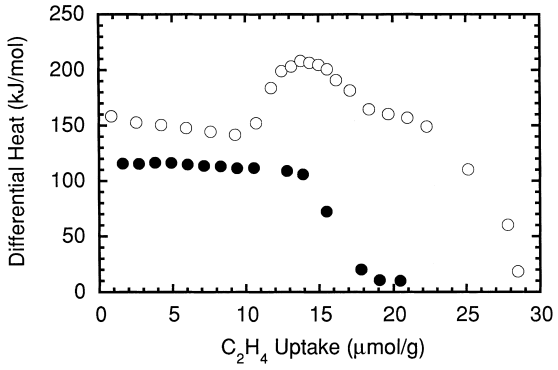

Fig. 7. Differential heats of ethylene adsorption on platinum powder [○, 303 K; and ●, 173 K].

negative of the enthalpy change of adsorption per mole of gas adsorbed. This figure shows an initial heat of 93 kJ/mol, in agreement with heats of 90 ± 5 kJ/mol reported for hydrogen adsorption on platinum powder [19], silica-supported platinum [11,21,29,30], and zeolite-supported platinum [29]. Fig. 6 shows that the differential heat of adsorption decreases gradually with increasing coverage, until the surface becomes saturated with hydrogen.

2.3. Studies of ethylene adsorption on platinum

The interactions of ethylene with single crystal platinum surfaces and with supported platinum catalysts have been widely studied, and the results of these investigations reveal the presence of distinct surface species depending on temperature. For example, ultrahigh vacuum studies of ethylene adsorption on Pt(111) have identified π-bonded ethylene species at temperatures below 52 K [31]; di-σ-bonded ethylene species from 100 to 250 K [32–34]; and ethylidyne species from 280 to 450 K [32,33,35]. Importantly, Sheppard and De La Cruz have shown in a recent review [36] that comparable results are obtained when ethylene is dosed onto supported platinum catalysts and onto platinum single crystal surfaces. For example, infrared spectra show the presence of π-bonded and di-σ-bonded species when ethylene is dosed onto silica- and alumina-supported platinum at low temperatures (<195 K), whereas ethylidyne species form at room temperature.

The strengths with which the aforementioned species interact with platinum powder have been probed microcalorimetrically, as shown in Fig. 7. Details of this microcalorimetric investigation are reported elsewhere [19]. This Fig. shows the differential heat for the associative adsorption of ethylene at 173 K and the dissociative adsorption of ethylene to form ethylidyne species at 303 K. At 303 K, ethylene adsorbs with an initial heat of 160 kJ/mol, in general agreement with heats of 150 ± 5 kJ/mol reported for ethylene adsorption on silica-supported platinum [20,21,30]. Fig. 7 shows that the differential heat apparently increases at higher coverages and then decreases until the surface becomes saturated. This apparent increase in heat is caused by the formation of gaseous ethane upon reaction of ethylene with surface hydrogen formed from the dissociative adsorption of ethylene to form ethylidyne species at lower coverages [19]. At 173 K, Fig. 7 shows that ethylene adsorbs on platinum powder with an initial heat of 120 kJ/mol. Studies of ethylene adsorption on Pt at temperatures between 100 and 270 K have shown that ethylene adsorbs associatively as di-σ-adsorbed species and/or a π-adsorbed species [36,37]. Accordingly, the observed heat of 120 kJ/mol in Fig. 7 can be attributed to formation of di-σ and π species on platinum [19]. Recently, similar initial heats of adsorption were observed for ethylene adsorption on silica-supported platinum at temperatures lower than 200 K [20]. Low temperature infrared spectroscopic investigations over the same Pt/SiO_2 showed that these observed heats may, in fact, be attributed to the formation of di-σ and π-adsorbed ethylene species [20].

In addition to the above microcalorimetric studies over platinum powder and supported platinum cata-

lysts, King and co-workers [38–40] have used ultra-high vacuum microcalorimetry to measure the heats of ethylene adsorption on platinum single crystals at 300 K. These investigators reported heats of ethylene adsorption to form four distinct surface species on Pt(110)(2x1): (1) a heat of 205 kJ/mol was attributed to the dissociation of two hydrogen atoms from ethylene to form a vinylidene (CCH_2) species on platinum; (2) a heat of 175 kJ/mol was caused by the dissociation of one hydrogen atom from ethylene and the formation of adsorbed ethylidyne (CCH_3) species; and (3) heats of 135 kJ/mol and 120 kJ/mol were caused by associative adsorption of ethylene to form di-σ-adsorbed and π-adsorbed species, respectively.

We have recently used quantum chemical methods, employing density functional theory (DFT), to predict the energetics of various C_2H_x(ads) species formed from the interaction of ethylene with a 10-atom platinum cluster [22]. Such DFT methods have proven to be useful to predict geometries and energetics for molecules containing transition metals [41–45]. The currently available DFT methods use few semi-empirical parameters in conjunction with more advanced functionals to give an adequate description of non-local effects in electron exchange and correlation interactions.

The results predicted from these theoretical calculations show good agreement (within 20 kJ/mol) with the experimental heats of adsorption obtained microcalorimetrically [22], as shown in Table 1. This agreement between predicted and experimental results demonstrates the utility of the theoretical calculations and gives an estimate of the confidence expected for prediction of structures and energetics of various hydrocarbon intermediates that cannot be examined by common experimental techniques. For example, Table 2 shows predictions for heats of interaction with Pt for various CH_x(ads) hydrocarbons that cannot be measured directly by calorimetric methods [22]. Additionally, this table shows heats of interaction of undetectable C_2H_x(ads) intermediates, such as adsorbed ethyl (C_2H_5) and ethylidene ($CHCH_3$) species. Accordingly, such predictions provide estimates of the energetics for formation of hydrocarbon fragments on surfaces that may play important roles in the elementary steps of ethane hydrogenolysis. Importantly, it was shown that the formation of C_2H_x(ads) species becomes more endothermic and the standard entropy change becomes more positive as more hydrogen atoms are removed from ethane [22]. Accordingly, the formation of more highly dehydrogenated C_2H_x(ads) species is favored with increasing temperature, and it was shown that CCH_2(ads) species are predicted to be the most abundant species on Pt at the typical reaction conditions for ethane hydrogenolysis used in the present study.

2.4. DFT studies of C–C bond dissociation

The generally good agreement between results predicted from quantum chemical calculations and results observed from experimental investigations (see Table 1) permits the extension of these theoretical methods to predict the structures and energies of transitions states involved in C–C bond dissociation of various C_2H_x(ads) species [22]. The location of transition states is a computationally difficult task, since it is necessary to calculate the Hessian matrix to confirm the existence of exactly one negative eigenvalue. Such calculations were made feasible by locating transition states using smaller metal clusters [22]. This approach used only those platinum atoms that are directly bonded to the carbon atoms of the hydrocarbon species in the reactant or the transition state. The Pt–Pt distance was frozen at its bulk value of 2.77 Å during the optimization of transition states and reactants. The small clusters were then embedded in 10 or 13 atom platinum clusters with fixed Pt–Pt distances. Single point energy calculations were then conducted on these clusters to estimate heats of reactions to form activated complexes for the various C–C bond cleavage reactions from gas-phase ethane, with the formation of gas-phase dihydrogen (see Step 4).

Table 3 shows the theoretically predicted activation energies for the formation of different activated complexes on both the Pt_{10} and Pt_{13} clusters. The results from these DFT calculations predict that the activated complexes based on the ethyl ($[C_2H_5Pt_x]^{\ddagger}$) and ethylidene ($[CHCH_3Pt_x]^{\ddagger}$) species are the most reactive intermediates for ethane hydrogenolysis. The activated complexes for the other reaction pathways exhibit considerably higher activation energies, because sufficient Pt–C bonds are not formed or because the C–C bond length is longer in these other activated complexes.

Table 1
Comparison of experimental and theoretical results

Reaction	Energy Change (kJ/mol)		
	DFT	Experimental	
	(ref. [22])	(ref. [38])	(ref. [19])
$Pt_{10} + C_2H_4 = Pt_{10}\text{-}C_2H_4$ (di-σ)	−171	−136	−120
$Pt_{10} + C_2H_4 = Pt_{10}\text{-}C_2H_4$ (π)	−103	−120	(di-σ + π species)
$Pt_{10} + C_2H_4 = Pt_{10}\text{-}CCH_3 + 0.5H_2$ (ethylidyne)	−127	−125	−115
$Pt_{10} + C_2H_2 = Pt_{10}\text{-}C_2H_2$ (di-σ/π)	−209		−210
$Pt_{10} + C_2H_2 = Pt_{10}\text{-}CCH_2$ (vinylidene)	−278	−290	

Table 2
DFT results for adsorption of C_1 and C_2 hydrocarbons species on Pt_{10} clusters [22]

Reaction	$\Delta E_{electronic}$	ΔH (298 K)	ΔH (623 K)
	(kJ/mol)	(kJ/mol)	(kJ/mol)
$Pt_{10} + C_2H_4 = Pt_{10}\text{-}C_2H_4$ (di-σ ethylene)	−149	−171	−166
$Pt_{10} + C_2H_4 = Pt_{10}\text{-}C_2H_4$ (π ethylene)	−103	−103	−103
$Pt_{10} + C_2H_4 = Pt_{10}\text{-}CCH_3 + 0.5H_2$ (ethylidyne)	−109	−127	−124
$Pt_{10} + C_2H_4 = Pt_{10}\text{-}CHCH_2 + 0.5H_2$ (vinyl)	−53	−78	−73
$Pt_{10} + C_2H_2 = Pt_{10}\text{-}C_2H_2$ (di-σ/π acetylene)	−209	−209	−209
$Pt_{10} + C_2H_2 = Pt_{10}\text{-}C_2H_2$ (π acetylene)	−88	−88	−88
$Pt_{10} + C_2H_2 = Pt_{10}\text{-}CCH_2$ (di-σ/π vinylidene)	−274	−278	−280
$Pt_{10} + CH_4 = Pt_{10}\text{-}CH + 1.5H_2$	102	54	64
$Pt_{10} + CH_4 = Pt_{10}\text{-}CH_2 + H_2$	118	81	88
$Pt_{10} + CH_4 = Pt_{10}\text{-}CH_3 + 0.5H_2$	6	−15	−10
$Pt_{10} + C_2H_6 = Pt_{10}\text{-}C_2H_5 + 0.5H_2$ (ethyl)	1	−20	−15
$Pt_{10} + C_2H_4 = Pt_{10}\text{-}CHCH_3$ (ethylidene)	−87	−95	−94

Table 3
Theoretical predictions of activation energies for C–C cleavage steps [23]

Reaction	$\Delta E_{electronic}$ (kJ/mol)		$\Delta G^{o\ddagger}$ (623 K) (kJ/mol)
	Pt_{10}	Pt_{13}	Pt_{13}
$C_2H_6 + Pt_x \rightleftharpoons [C_2H_5Pt_x]^{\ddagger} + 1/2H_2$	183	117	167
$C_2H_6 + Pt_x \rightleftharpoons [CHCH_3Pt_x]^{\ddagger} + H_2$	162	169	165
$C_2H_6 + Pt_x \rightleftharpoons [CH_2CH_2\ Pt_x]^{\ddagger} + H_2$	430	277	
$C_2H_6 + Pt_x \rightleftharpoons [CHCH_2Pt_x]^{\ddagger} + 3/2H_2$	256	292	
$C_2H_6 + Pt_x \rightleftharpoons [CCH_2Pt_x]^{\ddagger} + 2H_2$	360	346	

We also conducted DFT calculations to determine the vibrational frequencies of the activated complexes based on the ethyl and ethylidene species [23]. These vibrational frequencies may be used to determine 0-point and thermal corrections to the electronic energy as well as applied to determine the entropies of the transition states. These results allow the prediction of the standard free energy changes ($\Delta G^{o\ddagger}$) to form the activated complexes based on the ethyl ($[C_2H_5Pt_x]^{\ddagger}$) and ethylidene ($[CHCH_3Pt_x]^{\ddagger}$) species in equilibria with gaseous C_2H_6 and H_2, as shown in Table 3. This table shows the predicted standard free energy changes at 623 K for the two most favorable transition states on a Pt_{13} cluster, from which it can be seen that the free energy changes to form these two activated complexes are essentially equal.

Accordingly, the quantum chemical calculations predict that the preferred reaction pathways for ethane hydrogenolysis over platinum are through the activated complexes based on the ethyl and ethylidene species, and these calculations predict these two pathways to have similar rates.

3. Kinetic analyses

3.1. Reaction schemes

In view of the quasi-equilibrated formation of C_2H_x(ads) species with $2 \le x \le 5$ and C–C bond cleavage of C_2H_x(ads) species with $3 \le x \le 5$ expressed in Steps 1–3, we simplify the reaction scheme of Fig. 1 to a series of eight-lumped-equilibria. Accordingly, Steps 5 through 12 shown below were used for analysis of the ethane hydrogenolysis kinetic data.

Step 5 $H_2 + 2* \rightleftharpoons 2H*$

Step 6 $C_2H_6 + * \rightleftharpoons C_2H_5* + 1/2H_2$

Step 7 $C_2H_6 + 2* \rightleftharpoons C_2H_4*_2 + H_2$

Step 8 $C_2H_6 + 3* \rightleftharpoons C_2H_3*_3 + 3/2H_2$

Step 9 $C_2H_6 + 4* \rightleftharpoons C_2H_2*_4 + 2H_2$

Step 10 $C_2H_6 + 3* \rightleftharpoons [C_2H_5*_3]^{\ddagger} + 1/2\ H_2$

Step 11 $C_2H_6 + 4* \rightleftharpoons [CHCH_3*_4]^{\ddagger} + H_2$

Step 12 $C_2H_6 + 5* \rightleftharpoons [CHCH_2*_5]^{\ddagger} + 3/2\ H_2$

The overall rate of this reaction scheme is determined by summation of the rates from the three C–C cleavage steps:

$$\text{rate} = \frac{k_B T}{h}\left[\frac{K_5^{\ddagger} P_E \theta_*^3}{P_H^{1/2}} + \frac{K_4^{\ddagger} P_E \theta_*^4}{P_H} + \frac{K_3^{\ddagger} P_E \theta_*^5}{P_H^{3/2}}\right] \quad (7)$$

and the site balance is given by:

$$\theta_* = 1 - \theta_H - \theta_{C_2H_5*} - 2\theta_{C_2H_4*_2} - 3\theta_{C_2H_3*_3} - 4\theta_{C_2H_2*_4} \quad (8)$$

where the coverages of the stable species are given by Eqs. (9)–(13):

$$\theta_H = \sqrt{K_H P_H}\,\theta* \quad (9)$$

$$\theta_{C_2H_5*} = \frac{K_5 P_E \theta_*}{P_H^{1/2}} \quad (10)$$

$$\theta_{C_2H_4*_2} = \frac{K_4 P_E \theta_*^2}{P_H} \quad (11)$$

$$\theta_{C_2H_3*_3} = \frac{K_3 P_E \theta_*^3}{P_H^{3/2}} \quad (12)$$

$$\theta_{C_2H_2*_4} = \frac{K_2 P_E \theta_*^4}{P_H^2} \quad (13)$$

3.2. Parameterization of the kinetic model

The equilibrium constants required to describe coverages of stable surface species ($H*$, C_2H_5*, $C_2H_4*_2$, $C_2H_3*_3$, and $C_2H_2*_4$) are expressed in terms of the appropriate standard entropies (S_H^o, S_5^o, S_4^o, S_3^o, and S_2^o, respectively) and enthalpy changes (ΔH_H, ΔH_5, ΔH_4, ΔH_3, and ΔH_2, respectively). The reference pressure for the standard state is 1 atm. The standard entropy changes can be expressed in terms of known gaseous entropies and entropies of the appropriate surface species. Furthermore, the equilibrium constants for the formation of the activated complexes ($[C_2H_5*_3]^{\ddagger}$, $[CHCH_3*_4]^{\ddagger}$, and $[CHCH_2*_5]^{\ddagger}$) can also be expressed in terms of standard entropies ($S_5^{o\ddagger}$, $S_4^{o\ddagger}$, and $S_3^{o\ddagger}$) and enthalpy changes ($\Delta H_5^{\ddagger}$, $\Delta H_4^{\ddagger}$, and $\Delta H_3^{\ddagger}$). Standard entropies and enthalpies of gas phase components were determined from the reference of Stull et al. [46].

The number of adjustable parameters was reduced by fixing the values for the enthalpies changes to form adsorbed ethyl species, di-σ-adsorbed ethylene species and ethylidyne species at −25, 7, and 17 kJ/mol, respectively. These constrained values were determined from reported calorimetric results of King and co-workers [38] or determined from DFT calculations over a Pt_{10} cluster [22]. The entropy and enthalpy for adsorbed atomic hydrogen were fixed to average values determined over the investigated range of reaction conditions. In particular, the kinetic analyses show that the surface should be largely covered with atomic hydrogen and the average fraction of free sites should be 0.21. Results from our microcalorimetric studies of hydrogen adsorption on silica-supported

platinum indicate a heat of 62 kJ/mol and a surface entropy of 42 J/mol/K at this average coverage.

The surface entropies of C_2H_x(ads) species were linked together assuming that all stable species exhibit similar mobility on the surface. Accordingly, the fitting parameter for the surface entropies of C_2H_x(ads) species was a factor which multiplied the local surface entropies of these species when these species possess 0 degrees of translational freedom (S_{loc}). At 623 K, the values of S_{loc} for C_2H_5*, $C_2H_4*_2$, $C_2H_3*_3$, $C_2H_2*_4$ species are 105, 96, 85, and 74 J/mol/K, respectively. In a similar manner, the entropies for the activated complexes were linked together assuming that these species exhibit the same mobility on the surface. The value of the multiplicative factor for the ratio of $S_x^{\ddagger}$ to $S_{x\,(loc)}$ was fixed at 0.95, which is the value determined from DFT frequency calculations for the activated complexes [23]. Accordingly, the reaction kinetic data were fit in terms of five parameters, $\Delta H_5^{\ddagger}$, $\Delta H_4^{\ddagger}$, and $\Delta H_3^{\ddagger}$, ΔH_2, and the single multiplicative factor that gives S_x in terms of $S_{x\,(loc)}$. It was found necessary to vary ΔH_2, since $C_2H_2*_4$ species were initially predicted to be too highly abundant on the surface (since Step 9 has a large positive standard entropy change) [22]. Values for the five fitted parameters were determined using a general regression analysis of the reaction kinetics data, with the reactor treated as a CSTR. All values of the parameters were estimated at the average reactor temperature of 623 K.

The solid lines shown in Figs. 2–5 represent the rates of ethane hydrogenolysis predicted using the reaction scheme of Steps 5–12 and the parameters listed in Table 4. It can be seen in these figures that the kinetic model provides a good representation of the experimental data over the range of experimental conditions. Table 4 lists the values of the fixed and fitted parameters and the 95% confidence limits for the fitted parameters. The ratio between the values of surface entropies of the C_2H_x species and the values of S_{loc} for these species was found to be 1.1, which suggests that these adsorbed species are essentially immobile on the surface.

The kinetic analyses indicate that the major reaction pathways proceed through the activated complex based on the ethylidene ($CHCH_3$) species, followed by the activated complex based on the ethyl (C_2H_5) species. Over our range of reaction conditions, the ethylidene pathway accounted for 67% of the observed rate while the ethyl pathway accounted for the remaining 33% of the observed rate. The analyses suggest that the reaction pathway through the more highly dehydrogenated activated complex $[CHCH_2*_5]^{\ddagger}$ is not significant. Accordingly, our constrained kinetic model requires only four fitted parameters to adequately describe the observed kinetic results.

Table 4
Parameters for ethane hydrogenolysis over Pt/SiO_2

Parameter	Value (J/mol/K)	Parameter	Value (kJ/mol)
S_{H*}	42 fixed	ΔH_H	−62 fixed
$S_{C_2H_5*}$	116[a]	ΔH_5	−15 fixed
$S_{C_2H_4*_2}$	106[a]	ΔH_4	7 fixed
$S_{C_2H_3*_3}$	94[a]	ΔH_3	17 fixed
$S_{C_2H_2*_4}$	82[a]	ΔH_2	72 ± 25
$S_{C_2H_5^{\ddagger}}$	100.5[b]	$\Delta H_5^{\ddagger}$	77 ± 2
$S_{CHCHH_3^{\ddagger}}$	91.6[b]	$\Delta H_4^{\ddagger}$	110 ± 2
$S_{CHCHH_2^{\ddagger}}$	81.0[b]	$\Delta H_3^{\ddagger}$	271 (insensitive)

[a] Fitted parameter was ratio of surface entropy to S_{loc} for a given surface species. This value of this parameter was found to be 1.10 ± 0.02.

[b] The fitting parameter was the ratio of surface entropy of the activated complex to S_{loc} for a given surface species. This parameter was fixed at 0.95 as indicated from frequency calculations conducted on the activated complex [23].

It is noteworthy that the primary pathways for C–C bond cleavage take place through activated complexes that are rather highly hydrogenated (e.g., $CHCH_3$, C_2H_5) compared to the most abundant surface intermediates (e.g., CCH_2, C_2H_3). Accordingly, the C_2H_x(ads) reactive species that are responsible for C–C bond cleavage are not necessarily the most abundant surface intermediates that could be observed spectroscopically. However, these most abundant surface intermediates still play an important role in the reaction kinetics by determining the fraction of the surface that is available for catalytic reaction (i.e., they participate in site blocking).

4. Conclusions

The objective of this work was to develop a quantitative description of the catalytic chemistry for ethane hydrogenolysis over platinum that is consistent with results from a variety of experimental and theoreti-

cal investigations. Figs. 2–5 show that the predicted turnover frequencies based on Steps 5–12 are in good agreement with experimental values observed over a wide range of reaction conditions. Furthermore, the values of the parameters shown in Table 4 are physically reasonable and are in general agreement with experimental and theoretical results.

The above analyses suggest that while the most abundant surface species are not the reactive intermediates involved in major pathways for cleavage of the C–C bond, these abundant species influence the kinetic data through blocking effects. The entropy and enthalpy changes shown in Table 4 for Steps 6–9 indicate that the formation of C_2H_x(ads) species becomes more endothermic and the change in entropy increases as more hydrogen atoms are removed from ethane. Accordingly, the formation of the more highly dehydrogenated C_2H_x(ads) species is favored with increasing temperature. Therefore, vinylidene (CCH_2) species appear to become predominant on the surface, since these species involve removal of the most hydrogen atoms, resulting in a large positive standard entropy change. The parameters listed in Table 4 predict on average that 9% of the surface sites are covered by the C_2H_x(ads) hydrocarbon species (mostly ethylidyne and vinylidene species), 70% of the surface is covered by atomic hydrogen, with the remaining 21% of the sites being vacant over our range of reaction conditions.

It is recognized that there are limitations of the cluster approach applied in the theoretical calculations. Accordingly, microcalorimetric and spectroscopic results were applied to calibrate the theoretical methods by comparing results for observable stable surface intermediates, as shown in Table 1. The calibrated theoretical methods were then applied to estimate structures and energetics for reactive species that cannot be readily observed [22] as well as for transitions states involved in C–C bond cleavage of various C_2H_x(ads) species [22]. While the results of these theoretical calculations may not be highly quantitative, these calculations provide a strategy for estimating values for energetic parameters that are necessary to conduct kinetic analyses of reaction schemes.

Importantly, the results from the kinetic analyses of the experimental data are in general agreement with the theoretical calculations and suggest that the reaction pathways do not necessarily proceed through observable stable intermediates such as di-σ-bonded ethylene, ethylidyne species, or vinylidene species. Instead, it appears that ethane hydrogenolysis takes place primarily through less-stable adsorbed ethyl and ethylidene species, since quantum chemical calculations predict that the major C–C cleavage pathways are via the activated complexes based on ethyl (C_2H_5) and ethylidene ($CHCH_3$) species, as shown it Table 3. This conclusion is independent of the energetics and mobilities of adsorbed atomic hydrogen and the various C_2H_x(ads) reaction intermediates, since these species are in quasi-equilibrium with gaseous C_2H_6 and H_2.

In general, the combination of results from diverse experimental studies and theoretical calculations forms an effective approach to estimate reasonable energetics for proposed reaction pathways. Subsequent analysis of reaction kinetics data collected over a wide range of conditions provides a feasibility test of the proposed reaction scheme. A quantitative description of the available experimental and theoretical results may then be used to guide further research and/or development of the catalytic system.

Acknowledgements

We acknowledge financial support for the experimental work of this research by the National Science Foundation and financial support for the modeling work of this research by the National Center for Clean Industrial and Treatment Technologies. We thank Professor W.E. Stewart for providing us with his general regression analysis software (GREG) and Rod Bain for providing us with his non-linear equation solver (NNES).

References

[1] J.H. Sinfelt, W.F. Taylor, D.J.C. Yates, J. Phys. Chem. 69(1) (1965) 95.
[2] J.H. Sinfelt, D.J.C. Yates, J. Catal. 8 (1967) 82.
[3] J.H. Sinfelt, J. Catal. 27 (1972) 468.
[4] J.H. Sinfelt, Adv. Catal. 23 (1973) 91.
[5] A. Cimino, M. Boudart, H.S. Taylor, J. Phys. Chem. 58 (1954) 796.
[6] G.C. Bond, M.R. Gelsthorpe, Faraday Trans. I 85(11) (1989) 3767.
[7] G.C. Bond, R.H. Cunningham, J. Catal. 163 (1996) 328.

[8] G.C. Bond, A.D. Hooper, J.C. Slaa, A.O. Taylor, J. Catal. 163 (1996) 319.
[9] G.C. Bond, R.H. Cunningham, J. Catal. 166 (1997) 172.
[10] G.C. Bond, R.H. Cunningham, E.L. Short. Kinetics of Alkane Hydrogenolysis on Clean and Coked Platinum and Platinum-Rhenium Catalysts, in: 10th International Congress on Catalysis, l992, Hungarian Academy of Sciences, Budapest, Hungary
[11] S.A. Goddard, M.D. Amiridis, J.E. Rekoske, N. Cardona-Martinez, J.A. Dumesic, J. Catal. 117 (1989) 155.
[12] L. Guczi, K. Matusek, M. Eszterle, J. Catal. 60 (1979) 121.
[13] B.S. Gudkov, L. Guczi, P. Tétényi, J. Catal. 1982 (1982) 207.
[14] S. Kristyan, J. Szamosi, J. Chem. Soc., Faraday Trans. 1 80 (1984) 1645.
[15] R. Larsson, Cat. Lett. 13 (1992) 71.
[16] S.B. Shang, C.N. Kenney, J. Catal. 134 (1992) 134.
[17] C.A. Klug, C.P. Slichter, Israel J. Chem. 32 (1992) 185.
[18] F. Zaera, G.A. Somorjai, J. Phys. Chem. 89 (1985) 3211.
[19] B.E. Spiewak, R.D. Cortright, J.A. Dumesic, J. Catal. 176 (1998) 405.
[20] J. Shen, J.M. Hill, R.M. Watwe, B.E. Spiewak, J.A. Dumesic, J. Phys. Chem., 1998, in press
[21] R.D. Cortright, J.A. Dumesic, J. Catal. 148 (1994) 771.
[22] R.M. Watwe, B.E. Spiewak, R.D. Cortright, J.A. Dumesic, J. Catal. 180 (1998) 184.
[23] R.M. Watwe, R.D. Cortright, J.K. Nørskov, J.A. Dumesic (1999), submitted to J. Phys. Chem. B.
[24] H.A. Benesi, R.M. Curtis, H.P. Studer, J. Catal. 10 (1968) 328.
[25] J.B. Anderson, Chem. Eng. Sci. 18 (1963) 147.
[26] D.E. Mears, Ind. Eng. Chem. Process Des. Develop. 10(4) (1971) 541.
[27] D.E. Mears, J. Catal. 20 (1971) 127.
[28] B. Sen, M.A. Vannice, J. Catal. 130 (1991) 9.
[29] S.B. Sharma, J.T. Miller, J.A. Dumesic, J. Catal. 148 (1994) 198.
[30] N.A. Natal-Santiago, S.G. Podkolzin, R.D. Cortright, J.A. Dumesic, Cat. Lett. 45 (1997) 155.
[31] A. Cassuto, J. Kiss, J.M. White, Surf. Sci. 255 (1991) 289.
[32] P. Cremer, C. Stanners, J.W. Niemantsverdriet, Y.R. Shen, G. Somorjai, Surf. Sci. 328 (1995) 111.
[33] J.E. Demuth, Surf. Sci. 80 (1979) 367.
[34] H. Ibach, S. Lehwald, J. Vac. Sci. Technol. 15(2) (1979) 407.
[35] L.L. Kesmodel, L.H. Dubois, G.A. Somorjai, J. Chem. Phys. 70(5) (1979) 2180.
[36] N. Sheppard, C. De La Cruz, Adv. Catal. 41 (1996) 1.
[37] N. Sheppard, Ann. Rev. Phys. Chem. 39 (1988) 589.
[38] A. Stuck, C.E. Wartnaby, Y.Y. Yeo, D.A. King, Phys. Rev. Lett. 74(4) (1995) 578.
[39] Y.Y. Yeo, C.E. Wartnaby, D.A. King, Science 268 (1995) 1731.
[40] Y.Y. Yeo, A. Stuck, C.E. Wartnaby, D.A. King, Chem. Phys. Lett. 259 (1996) 28.
[41] A. Fahmi, R.A. van Santen, J. Phys. Chem. 100 (1996) 5676.
[42] P.E.M. Siegbahn, Adv. Chem. Phys. XCIII, 1996, 333.
[43] R.A. van Santen, M. Neurock, Catal. Rev. Sci. Eng. 37(4) (1995) 557.
[44] R.A. van Santen, J.W. Niemantsverdriet, Chemical kinetics and catalysis, in: M.V. Twigg, M.S. Spencer (Ed.), Fundamental and Applied Catalysis, Plenum Press, New York, 1995.
[45] R.A. van Santen. Theory of hetero using cluster approximation, in: NATO ASI Series E: Applied Sciences – Chemisorption and Reactivity on Supported Clusters and Thin Films, 1996, Kluwer Academic Publishers, Erice, Trapani, Sicily.
[46] D.R. Stull, J.E.F. Westrum, G.C. Sinke, in: The Chemical Thermodynamics of Organic Compounds, Wiley, 1969, 865.